Nano Research

Open Access

Research Article

Large strain tunability of excitons in $ZrSe_3$ via cryogenic environment

Hao Li[1,§], Yu Hua[1,2,§], Jiaru Zhou[1,2], Gang Wang[3], Geng Li[1,2], Xiaofeng Fan[4], Changzhi Gu[1,2], and Baoli Liu[1,2] ✉

[1] *Beijing National Laboratory for Condensed Matter Physics, Institute of Physics, Chinese Academy of Sciences, Beijing 100190, China*
[2] *School of Physical Sciences, CAS Key Laboratory of Vacuum Physics, University of Chinese Academy of Sciences, Beijing 100190, China*
[3] *Key Laboratory of Advanced Optoelectronic Quantum Architecture and Measurement, Ministry of Education, School of Physics and Beijing Key Lab of Nanophotonics and Ultrafine Optoelectronic Systems, Beijing Institute of Technology, Beijing 100081, China*
[4] *Key Laboratory of Automobile Materials (Jilin University), Ministry of Education, and College of Materials Science and Engineering, Jilin University, Changchun 130012, China*
§ *Hao Li and Yu Hua contributed equally to this work.*

Cite this article: *Nano Research*, **2026**, *19*, 94908438. https://doi.org/10.26599/NR.2026.94908438

ABSTRACT: Strain engineering provides an efficient approach for tailoring the electronic and optical properties of two-dimensional (2D) materials, making them suitable candidates for straintronic applications, especially flexible optoelectronic devices. Therefore, the larger strain response on bandgap of 2D materials is highly on demand. Here, we systematically investigated the change of bandgap of multilayer IV–V transition metal trichalcogenide $ZrSe_3$, which is transferred onto flexible polycarbonate substrates, through the differential reflectance spectroscopy. A pronounced redshift of excitonic peak is observed with the applied biaxial compressive strain on multilayer $ZrSe_3$ through cryogenic cooling. A gauge factor of ~ 136 meV/%, which is the featured parameter related to strain response, is obtained. This value is comparable with the highest strain response reported among 2D materials to date. The exceptional strain tunability highlights $ZrSe_3$ as a promising material for flexible photodetectors and provides new insights into the manipulation of optical properties in 2D materials.

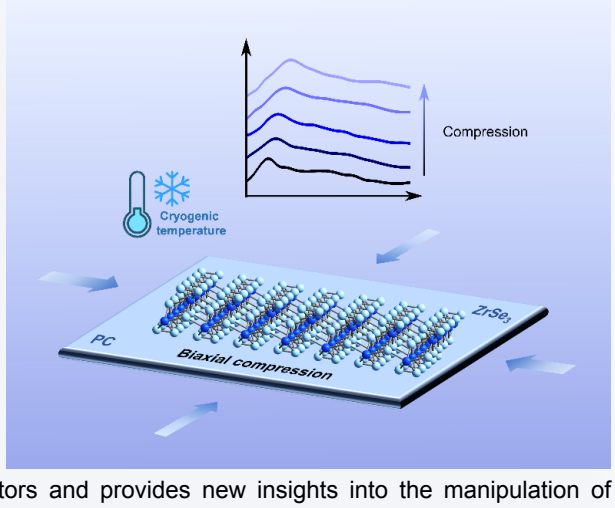

KEYWORDS: two-dimensional (2D) materials, strain, exciton, differential reflectance spectroscopy

1 Introduction

Straintronics, a branch of nanoelectronics, exploits mechanical strain to modify the electronic and optical properties of semiconductor materials, especially two-dimensional (2D) van der Waals materials. This approach provides a strategy to optimize device performance with reduced energy consumption and simplified fabrication route. The fundamental principle of straintronics involves the employment of mechanical deformation, which has emerged as a powerful tool towards tailoring the optical, electronic, vibrational, and magnetic properties of 2D materials [1–6]. Owing to their atomically thin nature, 2D materials are able to sustain ultrahigh strains without compromising the structure stability [7–9]. Furthermore, 2D materials present rather intrinsic strain-sensitive band structures, which offers an extraordinary manipulation feasibility on the bandgap that determines their electrical and optical properties [10–13]. This characteristic endows them superior suitability for straintronics, showing considerable potential application such as wearable bioelectronic devices, stretchable sensors, and flexible optoelectronic devices especially photodetectors [14–19]. Most of investigations have been focused on the strain engineering of transition metal dichalcogenides (TMDCs) such as MoS_2, WS_2, $MoSe_2$, and WSe_2 due to their high sensitivity to mechanical deformation [20–25]. Recently, the IV–V transition metal trichalcogenides (TMTCs) have been paid attention in the field of straintronics due to the orientation-resolved response to strain [26–31]. TMTCs exhibit the quasi-one-

Received: October 29, 2025
Accepted: January 13, 2026

✉Address correspondence to blliu@iphy.ac.cn

dimensional (1D) electrical and optical properties which originate from a reduced in-plane structural symmetry [32]. As a member of group TMTCs, the multi-layer $ZrSe_3$ presented a larger gauge factor of 60–95 meV/% under the uniaxial tensile strain applied along crystallographic *b* axis [33]. This gauge factor is 2–3 times larger than that in MoS_2 with the same strain strategy [34], which demonstrates an enhanced band structure regulation. This characteristic offers $ZrSe_3$ material the potential on straintronics since large strain response leads to ultrahigh sensitivity and responsivity [35, 36]. Despite the relatively-high strain response of $ZrSe_3$ induced by uniaxial strain has been studied, the biaxial strain on the multi-layer $ZrSe_3$ is not investigated up to now.

In this work, we apply biaxial compressive strain to high-quality multi-layer $ZrSe_3$ flakes (hereinafter referred to as $ZrSe_3$ flakes), which are transferred onto flexible polycarbonate (PC) substrate, by cooling down the $ZrSe_3$ flakes to cryogenic temperatures. The differential reflectance spectroscopy was utilized to probe the compressive strain-tuned exciton peak in multi-layer $ZrSe_3$ with the change of sample temperature. Remarkably, a dramatic redshift of exciton peak in $ZrSe_3$ flake was observed at lower temperature of ~ 13 K. The extracted gauge factor is about ~ 136 meV/% which is comparable with the highest strain response on 2D materials to date. This result exhibits an exceptional strain tunability on the excitons as well as the band structure in multilayer $ZrSe_3$.

2 Sample fabrication and straining strategy

Figure 1(a) shows the fabrication method of the $ZrSe_3$ flakes, which are mechanically exfoliated from bulk $ZrSe_3$ crystals and then transferred onto PC and Si/SiO_2 substrates [37]. Here two types of samples are denoted as PC-based and Si-based $ZrSe_3$ samples, respectively. Figure 1(b) shows an optical image of a representative PC-based $ZrSe_3$ flake in which the red dashed circle marks the region from which all the reflectance spectra are collected.

To apply biaxial compressive strain, PC-based $ZrSe_3$ flakes were cooled down from room temperature to ~ 13 K with a step of ~ 25 K, as schematically illustrated in Fig. 1(c). The reflectance spectra of the samples were collected at each temperature step to monitor the exciton energy of $ZrSe_3$. It is worth to note that both of the thermal effect and the strain can contribute to the observed change of the band structure under cryogenic conditions. In order to disentangle these two effects, the control experiments on Si-based $ZrSe_3$ samples were performed since the cooling process barely introduced the strain due to the rigidity of Si substrate. This comparison enables us to isolate the contribution of strain to the exciton energy of PC-based $ZrSe_3$ samples.

For PC-based $ZrSe_3$ samples, the thermal compression of PC, which produce the biaxial strain on $ZrSe_3$ flakes, is determined by the shrinkage of PC substrate due to decreased temperature. In order to calibrate the strain induced by the PC shrinkage, an array of photoresist pillars is fabricated on the surface of polycarbonate (PC) by electron beam lithography. And then, the PC substrate with pillar array was put into cryogenic environment. As shown in Figs. 2(a) and 2(b), the distance between the center points of the first and the final pillars at diagonal sites was measured by quantitative analysis of optical microscopy images with Gwyddion software. The shrinkage ε of PC can be expressed as Eq. (1)

$$\varepsilon(\%) = \frac{L - L_0}{L_0} \tag{1}$$

where L_0 and L represent the length of PC substrate at room temperature (295 K) and a specific temperature, respectively. A fit to a polynomial expression is used to correlate PC shrinkage ε and temperature T as presented in Fig. 2(c)

$$\varepsilon(\%) = -1.365 \times 10^{-8} T^3 + 1.132 \times 10^{-5} T^2 + 1.714 \times 10^{-3} T - 1.139 \tag{2}$$

which is in a good agreement with previous study [38].

3 Results and discussion

Figures 3(a) and 3(b) present the differential reflectance spectra of PC-based and Si-based $ZrSe_3$ samples with various temperatures from ~ 295 to ~ 13 K, respectively. The polarization direction of the incident supercontinuum laser is parallel to the b axis of $ZrSe_3$ flakes (See Figure S1 for the determination of b axis of $ZrSe_3$ flakes in Electronic Supplementary Material (ESM)). Here, the number of layers for both PC-based and Si-based $ZrSe_3$ flakes are 11 and 19, respectively (see Fig. 1(b) and Fig. S2 in the ESM for the

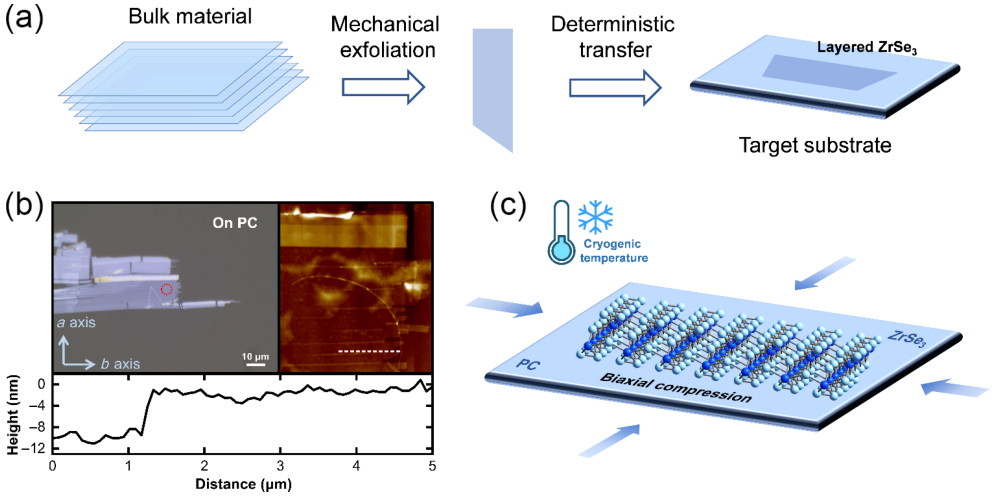

Figure 1 Graphic illustration of sample fabrication. (a) Deposition of layered $ZrSe_3$ flake on target substrate by deterministic transfer method. (b) Optical photo and AFM topography image of $ZrSe_3$ on PC substrate. Line profile measured along the white dash line in AFM image shows the thickness of the flake. (c) Illustration of biaxial compressive strain subjected on PC-based $ZrSe_3$ sample under cryogenic environment. Optical photos are collected under 50× objective. The scale bar is ~ 10 μm and the red dashed circle represents the laser spot in the following spectroscopy measurements.

measurements of number of layers). It is clear that both spectra present the distinct exciton peaks due to resonance absorption.

For PC-based $ZrSe_3$, the exciton energy (center position of peak) exhibits an abnormally dramatic redshift when the temperature of sample is cooled down from ~295 to ~13 K as shown in Fig. 3(a). On the contrary, for Si-based $ZrSe_3$, the exciton energy presents a blueshift characteristic of traditional semiconductor materials with decreased temperature down to ~13 K as shown in Fig. 3(b). Therefore, it is concluded the redshift of exciton energy in PC-based $ZrSe_3$ results from the biaxial compressive strain applied on $ZrSe_3$ due to the shrinkage of PC substrate. In order to obtain the pure effect of strain in PC-based $ZrSe_3$, the influence of temperature should be considered because the cooling-down temperature of $ZrSe_3$, can produce the blueshift of exciton energy as observed in Si-based $ZrSe_3$. Figure 3(c) plots the curves of the temperature-dependent exciton energy shifts. The redshift of exciton energy is about $\Delta E_{PC} \approx 100$ meV for PC-based $ZrSe_3$, while the blueshift of exciton energy is about $\Delta E_{Si} \approx -56$ meV for Si-based $ZrSe_3$. Therefore, the change of exciton energy solely induced by the biaxial compressive strain is about $\Delta E_{strain} \approx 156$ meV calculated through the equation $\Delta E_{strain} = \Delta E_{PC} - \Delta E_{Si}$. Now, the gauge factor is introduced to describe the magnitude of exciton energy shift per unit shrinkage/strain. Utilizing Eq. (1), the shrinkage ε can be calculated easily. Figure 3(d) plots the corresponding exciton energy shift as a function of applied strain which is represented by the shrinkage ε. Significantly, a large gauge factor of ~136 meV/% for exciton can be yielded, to the best of our knowledge, which is comparable with the highest strain response on 2D materials to date.

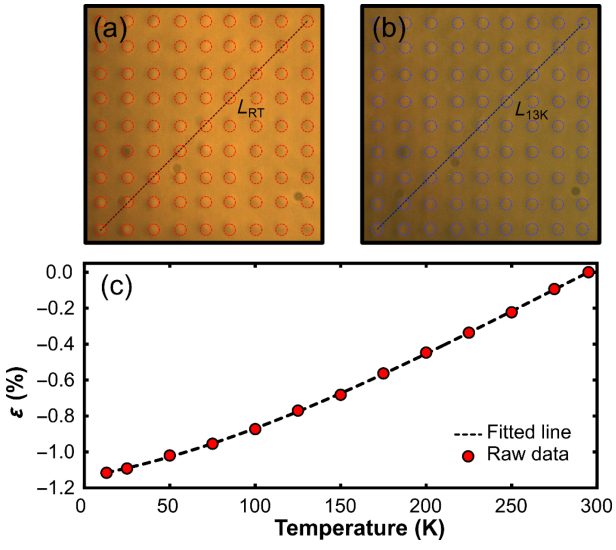

Figure 2 Optical images of a resist micropillars grid (~ 2 μm of diameter) on a polycarbonate substrate at (a) room temperature 295 K and (b) 13 K. The perimeter of each micropillar is delineated in red for 295 K and in blue for 13 K. (c) Average shrinkage ε (%) as a function of temperature. The dashed line represents a fitting of data by a polynomial function.

To access the feasibility of this strain-tuning strategy on the manipulation of exciton energy of $ZrSe_3$ flakes, the identical measurements of the differential reflectance spectroscopy are performed on 5 groups of $ZrSe_3$ flakes with the number of layers ranging from 10 to over 100 (see Figs. S3 to S10 in the ESM for the determination of layer number, note that flakes in each group are selected with similar layer numbers). Detailed differential reflectance spectroscopy results are presented in Figs. S11 to S14. Surprisingly, a markable gauge factor of ~ 80 meV/% was still observed even for flakes with layers over 100 (see Fig. S14 in the ESM), confirming that this type of strain engineering in $ZrSe_3$ remains effective even in thick flakes. Figure 4 shows the layer number-dependent gauge factors of 5 groups of $ZrSe_3$ samples. It is obvious that the gauge factor is linear-dependent on the thickness

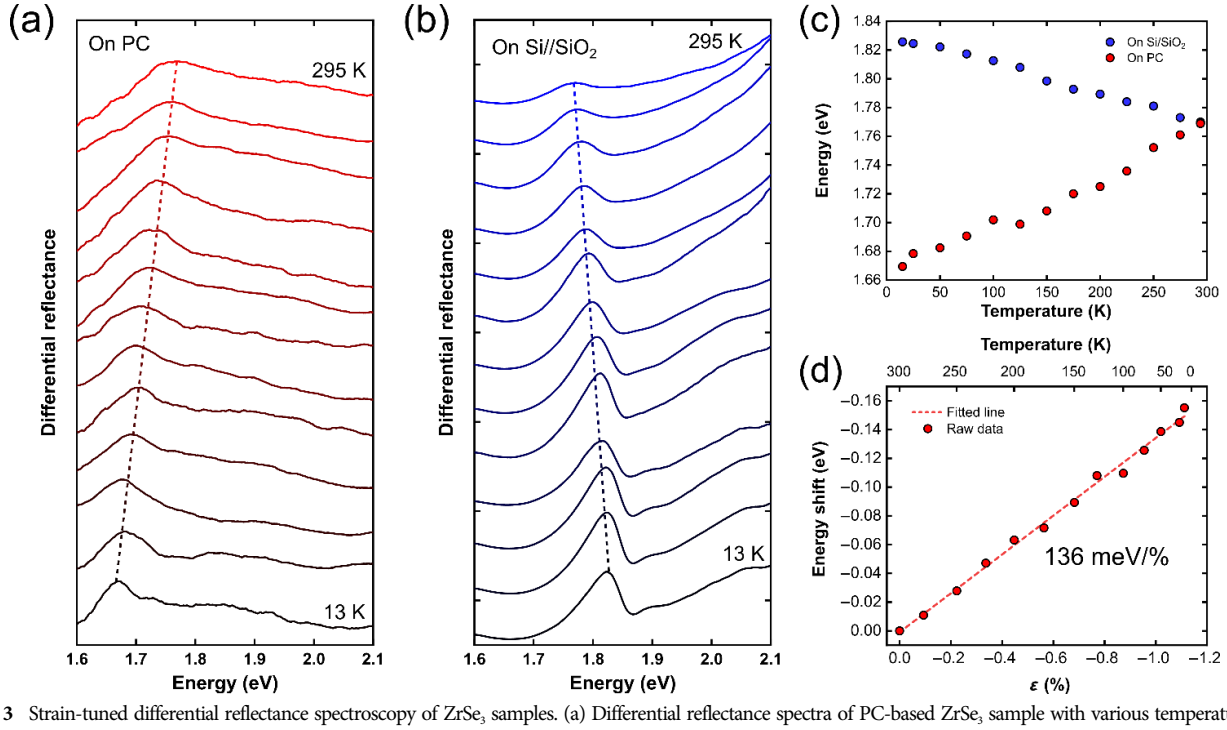

Figure 3 Strain-tuned differential reflectance spectroscopy of $ZrSe_3$ samples. (a) Differential reflectance spectra of PC-based $ZrSe_3$ sample with various temperature. (b) Differential reflectance spectra of Si-based $ZrSe_3$ sample with various temperatures. (c) The exciton energy as a function of the temperature obtained from (a) and (b). (d) Energy shift of exciton as a function of applied strain obtained from (c). A linear fit is employed to investigate the dependence of the energy shift on the applied strain.

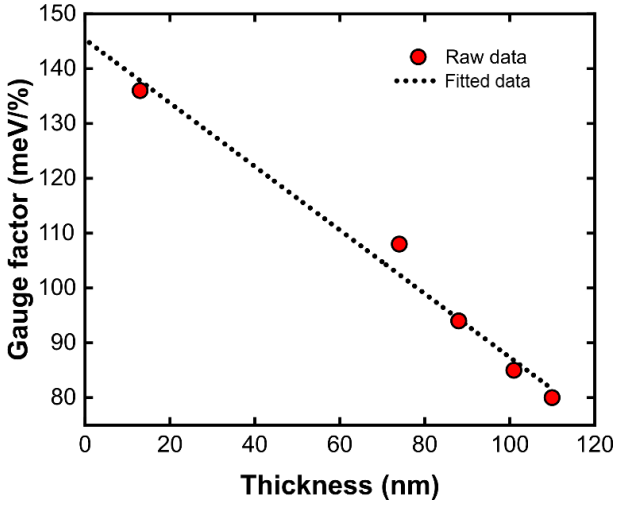

Figure 4 Layer number-dependent gauge factor of $ZrSe_3$ samples. A linear fit is employed to estimate the gauge factor of the monolayer $ZrSe_3$.

of $ZrSe_3$ flakes as presented by black dashed line in Fig. 4. A gauge factor of ~ 145 meV/% for monolayer (ML) $ZrSe_3$ was estimated through the extrapolation method. Please note that the ML $ZrSe_3$ cannot be fabricated up to now.

As an in-plane anisotropic material, the crystalline structure of $ZrSe_3$ is quite different along various orientations. Therefore, strain's effect on the band structure of $ZrSe_3$ along different crystalline orientations are apparently distinct [33, 39]. In previous study, theoretical simulation has revealed that contributions to the band structure depend on Zr and two Se atoms in the unit cell, where Se_2 atom is more internal and binds the two Zr atoms. While Se_1 is one of the external atoms that binds to the multilayer structure via van der Waals forces. In the aspect of band structure, conduction bands, around Γ, are mainly determined by the Zr d_{xy} and d_{yz} orbitals. Thus, deformation along *b* axis might introduce a more significant impact since it modifies the bonds containing the d_{xy} and d_{yz} orbitals. Meanwhile, deformation along *a* axis only perturbs the d_{xz} orbital which barely affects the conduction band. On the other hand, the valence band maximum around the Γ point is dominated by the p_z orbital of Se_2 atoms, which are relatively insensitive to strain along either direction [33]. Consequently, uniaxial tensile strain has proven to effectively elevate the valence band and thus, enlarge the bandgap at Γ point, leading to a blueshift in exciton. In contrast, the biaxial compressive strain was employed on PC-based $ZrSe_3$ under cryogenic condition, which reduces the valence band, further giving rise to a redshift of A exciton in $ZrSe_3$. Basically, the biaxial strain results in the excitonic redshift of $ZrSe_3$ via PC shrinkage in cryogenic condition, while the decreasing temperature generally brings up a prominent blueshift of exciton energy in various semiconductor materials [38, 40]. The combined effect of biaxial compression and cryogenic temperature is the origin of the exceptionally high gauge factor observed in $ZrSe_3$ in this work.

In fact, the biaxial strain induced by cryogenic temperature manipulates not only the optical properties, but also the electrical properties of 2D materials, for instance, the enhancement of the superconducting critical temperature [41] and the modulation of superconducting phase transition [42]. Those works demonstrated that the biaxial strain can act as a powerful method for extreme strain tunability in 2D materials with the condition of cryogenic temperature.

4 Conclusions

In summary, we have investigated strain-induced exciton modulation in layered $ZrSe_3$ under cryogenic conditions. Herein, biaxial compressive strain was introduced by transferring $ZrSe_3$ flake onto polycarbonate substrate and cooling the samples to low temperature. Furthermore, the measurements of differential reflectance spectroscopy were performed to study the strain-tuned exciton characteristics of $ZrSe_3$. Pronounced redshift of excitonic resonances in $ZrSe_3$ on PC was observed, revealing excellent tunability of strain on the excitons. Remarkably, a large gauge factor of ~136 meV/% was achieved under biaxial compressive strain with low temperature, being comparable with the largest strain response reported for 2D material to date. These findings establish $ZrSe_3$ as a highly strain-sensitive anisotropic semiconductor and pave an avenue for band structure engineering in 2D materials, offering significant potential for next-generation straintronic applications, especially flexible optoelectronic devices.

5 Experimental section

5.1 Sample fabrication

Bulk $ZrSe_3$ crystals (from 2D semiconductors company) were exfoliated with Nitto SPV 224 tape and transferred to a Gel-Film (Gel-Pak WF × 4 6.0 mil) substrate. Afterwards, the Gel-Film substrate with $ZrSe_3$ flakes was scanned under a 40× optical objective (Nikon company) operated in reflection mode to take a preliminary identification of the flakes. Once the desired flake was identified, it could be transferred onto a certain location of a target substrate by means of an all-dry deterministic placement method. Here, the flakes were transferred onto polycarbonate substrate (purchased from Tiannuo Company, China) and silicon wafer with 285 nm SiO_2.

5.2 Strain calibration

Pure PC substrate is patterned with photoresist pillars by electron beam lithography technique. Firstly, the PMMA photoresist was spin-coated on pure PC substrate with 1 cm × 1 cm size and further dried for 3 min under 90 °C, and then the conductive coating was spin-coated on it and further dried for 2 min Afterwards, the pattern of circular array with diameter of 2 μm was lithographed on the surface of PC substrate by electron beam lithography technique followed by developing and fixing processes. The strain was calibrated by placing the PC substrate with patterns into the cryogenic system and monitoring the displacement change between the diagonal photoresist pillars under various temperature ranging from 13 to 295 K with an interval of 25 K.

5.3 Low-temperature differential reflectance spectroscopy

The substrate containing the desired flake was loaded on the sample stage located inside of the vacuum chamber of Cryostation system (Montana instrument company) and the whole cryogenic system was integrated with a 40× objective (Nikon) and a fiber-coupled CCD spectrometer (Maya2000 pro, Ocean Optics company). For differential reflectance spectroscopy measurements, supercontinuum white laser source (SC PRO M, YSL photonics company) was used to illuminate $ZrSe_3$ samples with a power of 0.5 μW and the light was polarized to illuminate parallel to *b* axis of $ZrSe_3$ for obtaining strongest peak signal. Acquisition parameters are as follows: acquisition time: 50 ms; average time: 5; temperature:

13 to 295 K. The samples were measured under vacuum condition with temperature variation ranging from 13 to 295 K and the reflectance spectrums were collected per 25 K. Schematic diagram of optical measurement system is presented as Fig. 1(b) in Ref. [43].

Electronic Supplementary Material: Supplementary material is available in the online version of this article at https://doi.org/10.26599/NR.2026.94908438.

Data availability

All data needed to support the conclusions in the paper are presented in the manuscript and the Electronic Supplementary Material. Additional data related to this paper may be requested from the corresponding author upon request.

Acknowledgements

This work was supported by the National Key Research and Development Program of China (Nos. 2024YFA1207700, 2021YFA1400700, and 2022YFA1204100), the National Natural Science Foundation for Young Scientists of China (No. 12404042), China Postdoctoral Science Foundation (No. GZC20241892), and the Strategic Priority Research Program of Chinese Academy of Sciences (CAS) (No. XDB33020200).

Declaration of competing interest

All the contributing authors report no conflict of interests in this work.

Author contribution statement

H. L.: Data curation, investigation, formal analysis, writing manuscript, experimental design, funding acquisition. Y. H.: Data curation, investigation, formal analysis, experimental design. J. R. Z.: Data curation, investigation. G. W.: Resources. G. L.: Resources. X. F. F.: Resources. C. Z. G.: Resources, funding acquisition. B. L L.: Project administration, resources, writing – review & editing, experimental design, supervision, funding acquisition. All the authors have approved the final manuscript.

Use of AI statement

None.

References

[1] Roldán, R.; Castellanos-Gomez, A.; Cappelluti, E.; Guinea, F. Strain engineering in semiconducting two-dimensional crystals. *J. Phys.: Condens. Matter* **2015**, *27*, 313201.

[2] Amorim, B.; Cortijo, A.; De Juan, F.; Grushin, A. G.; Guinea, F.; Gutiérrez-Rubio, A.; Ochoa, H.; Parente, V.; Roldán, R.; San-Jose, P. et al. Novel effects of strains in graphene and other two dimensional materials. *Phys. Rep.* **2016**, *617*, 1–54.

[3] Dai, Z. H.; Liu, L. Q.; Zhang, Z. Strain engineering of 2D materials: Issues and opportunities at the interface. *Adv. Mater.* **2019**, *31*, 1805417.

[4] Peng, Z. W.; Chen, X. L.; Fan, Y. L.; Srolovitz, D. J.; Lei, D. Y. Strain engineering of 2D semiconductors and graphene: From strain fields to band-structure tuning and photonic applications. *Light: Sci. Appl.* **2020**, *9*, 190.

[5] Du, L. J.; Hasan, T.; Castellanos-Gomez, A.; Liu, G. B.; Yao, Y. G.; Lau, C. N.; Sun, Z. P. Engineering symmetry breaking in 2D layered materials. *Nat. Rev. Phys.* **2021**, *3*, 193–206.

[6] Zhu, C. R.; Wang, G.; Liu, B. L.; Marie, X.; Qiao, X. F.; Zhang, X.; Wu, X. X.; Fan, H.; Tan, P. H.; Amand, T. et al. Strain tuning of optical emission energy and polarization in monolayer and bilayer MoS_2. *Phys. Rev. B* **2013**, *88*, 121301.

[7] Lee, C.; Wei, X. D.; Kysar, J. W.; Hone, J. Measurement of the elastic properties and intrinsic strength of monolayer graphene. *Science* **2008**, *321*, 385–388.

[8] Bertolazzi, S.; Brivio, J.; Kis, A. Stretching and breaking of ultrathin MoS_2. *ACS Nano* **2011**, *5*, 9703–9709.

[9] Castellanos-Gomez, A.; Poot, M.; Steele, G. A.; Van Der Zant, H. S. J.; Agraït, N.; Rubio-Bollinger, G. Elastic properties of freely suspended MoS_2 nanosheets. *Adv. Mater.* **2012**, *24*, 772–775.

[10] He, K. L.; Poole, C.; Mak, K. F.; Shan, J. Experimental demonstration of continuous electronic structure tuning via strain in atomically thin MoS_2. *Nano Lett.* **2013**, *13*, 2931–2936.

[11] Conley, H. J.; Wang, B.; Ziegler, J. I.; Haglund, R. F. Jr.; Pantelides, S. T.; Bolotin, K. I. Bandgap engineering of strained monolayer and bilayer MoS_2. *Nano Lett.* **2013**, *13*, 3626–3630.

[12] Hui, Y. Y.; Liu, X. F.; Jie, W. J.; Chan, N. Y.; Hao, J. H.; Hsu, Y. T.; Li, L. J.; Guo, W. L.; Lau, S. P. Exceptional tunability of band energy in a compressively strained trilayer MoS_2 sheet. *ACS Nano* **2013**, *7*, 7126–7131.

[13] Castellanos-Gomez, A.; Roldán, R.; Cappelluti, E.; Buscema, M.; Guinea, F.; Van Der Zant, H. S. J.; Steele, G. A. Local strain engineering in atomically thin MoS_2. *Nano Lett.* **2013**, *13*, 5361–5366.

[14] Gant, P.; Huang, P.; De Lara, D. P.; Guo, D.; Frisenda, R.; Castellanos-Gomez, A. A strain tunable single-layer MoS_2 photodetector. *Mater. Today* **2019**, *27*, 8–13.

[15] Choi, H.; Choi, J. S.; Kim, J. S.; Choe, J. H.; Chung, K. H.; Shin, J. W.; Kim, J. T.; Youn, D. H.; Kim, K. C.; Lee, J. I. et al. Flexible and transparent gas molecule sensor integrated with sensing and heating graphene layers. *Small* **2014**, *10*, 3685–3691.

[16] Yang, C. F.; Li, L. L.; Zhao, J. X.; Wang, J. J.; Xie, J. X.; Cao, Y. P.; Xue, M. Q.; Lu, C. H. Highly sensitive wearable pressure sensors based on three-scale nested wrinkling microstructures of polypyrrole films. *ACS Appl. Mater. Interfaces* **2018**, *10*, 25811–25818.

[17] Ma, Z.; Tian, Z. A.; Li, X.; You, C. Y.; Wang, Y. L.; Mei, Y. F.; Di, Z. F. Self-rolling of monolayer graphene for ultrasensitive molecular sensing. *ACS Appl. Mater. Interfaces* **2021**, *13*, 49146–49152.

[18] Kim, D. B.; Kim, J. Y.; Han, J.; Cho, Y. S. Strain engineering in power-generating and self-powered nanodevices. *Nano Energy* **2024**, *125*, 109551.

[19] Aftab, S.; Hegazy, H. H.; Kabir, F. Emerging trends in 2D flexible electronics. *Adv. Mater. Technol.* **2023**, *8*, 2201897.

[20] Niehues, I.; Schmidt, R.; Drüppel, M.; Marauhn, P.; Christiansen, D.; Selig, M.; Berghäuser, G.; Wigger, D.; Schneider, R.; Braasch, L. et al. Strain control of exciton-phonon coupling in atomically thin semiconductors. *Nano Lett.* **2018**, *18*, 1751–1757.

[21] Niehues, I.; Blob, A.; Stiehm, T.; De Vasconcellos, S. M.; Bratschitsch, R. Interlayer excitons in bilayer MoS_2 under uniaxial tensile strain. *Nanoscale* **2019**, *11*, 12788–12792.

[22] Christopher, J. W.; Vutukuru, M.; Lloyd, D.; Bunch, J. S.; Goldberg, B. B.; Bishop, D. J.; Swan, A. K. Monolayer MoS_2 strained to 1.3% with a microelectromechanical system. *J. Microelectromech. Syst.* **2019**, *28*, 254–263.

[23] Li, Z. W.; Lv, Y. W.; Ren, L. W.; Li, J.; Kong, L. G.; Zeng, Y. J.; Tao, Q. Y.; Wu, R. X.; Ma, H. F.; Zhao, B. et al. Efficient strain modulation of 2D materials via polymer encapsulation. *Nat. Commun.* **2020**, *11*, 1151.

[24] John, A. P.; Thenapparambil, A.; Thalakulam, M. Strain-engineering the Schottky barrier and electrical transport on MoS_2. *Nanotechnology* **2020**, *31*, 275703.

[25] Island, J. O.; Kuc, A.; Diependaal, E. H.; Bratschitsch, R.; Van Der

Zant, H. S. J.; Heine, T.; Castellanos-Gomez, A. Precise and reversible band gap tuning in single-layer $MoSe_2$ by uniaxial strain. *Nanoscale* **2016**, *8*, 2589–2593.

[26] Zhu, W. N.; Liang, L. B.; Roberts, R. H.; Lin, J. F.; Akinwande, D. Anisotropic electron-phonon interactions in angle-resolved Raman study of strained black phosphorus. *ACS Nano* **2018**, *12*, 12512–12522.

[27] Li, Y. Y.; Hu, Z. X.; Lin, S. H.; Lai, S. K.; Ji, W.; Lau, S. P. Giant anisotropic Raman response of encapsulated ultrathin black phosphorus by uniaxial strain. *Adv. Funct. Mater.* **2017**, *27*, 1600986.

[28] Zhang, G. W.; Huang, S. Y.; Chaves, A.; Song, C. Y.; Özçelik, V. O.; Low, T.; Yan, H. G. Infrared fingerprints of few-layer black phosphorus. *Nat. Commun.* **2017**, *8*, 14071.

[29] Luo, W. J.; Oyedele, A. D.; Gu, Y. Y.; Li, T. S.; Wang, X. Z.; Haglund, A. V.; Mandrus, D.; Puretzky, A. A.; Xiao, K.; Liang, L. B. et al. Anisotropic phonon response of few-layer $PdSe_2$ under uniaxial strain. *Adv. Funct. Mater.* **2020**, *30*, 2003215.

[30] Wang, Y. X.; Yao, S. K.; Liao, P. L.; Jin, S. Y.; Wang, Q. X.; Kim, M. J.; Cheng, G. J.; Wu, W. Z. Strain-engineered anisotropic optical and electrical properties in 2D chiral-chain tellurium. *Adv. Mater.* **2020**, *32*, 2002342.

[31] Fan, X. Y.; Shen, Z. L.; Hu, D.; Liu, Y. N.; Tang, T. H.; Yang, W. C.; Liu, H. Y.; Song, Y. X.; Wang, Q. S.; Liu, B. L. et al. Anisotropic phonon responses of 2D $NbOX_2$ (X=Cl, Br, I) under uniaxial tensile strain. *Appl. Phys. Lett.* **2025**, *126*, 062103.

[32] Li, L.; Han, W.; Pi, L. J.; Niu, P.; Han, J. B.; Wang, C. L.; Su, B.; Li, H. Q.; Xiong, J.; Bando, Y. et al. Emerging in‐plane anisotropic two-dimensional materials. *InfoMat* **2019**, *1*, 54–73.

[33] Li, H.; Sanchez-Santolino, G.; Puebla, S.; Frisenda, R.; Al-Enizi, A. M.; Nafady, A.; D'Agosta, R.; Castellanos-Gomez, A. Strongly anisotropic strain-tunability of excitons in exfoliated $ZrSe_3$. *Adv. Mater.* **2022**, *34*, 2103571.

[34] Carrascoso, F.; Li, H.; Frisenda, R.; Castellanos-Gomez, A. Strain engineering in single-, bi- and tri-layer MoS_2, $MoSe_2$, WS_2 and WSe_2. *Nano Res.* **2021**, *14*, 1698–1703.

[35] Mumtaz, F.; Roman, M.; Zhang, B. H.; Abbas, L. G.; Ashraf, M. A.; Dai, Y. T.; Huang, J. Highly sensitive strain sensor by utilizing a tunable air reflector and the vernier effect. *Sensors* **2022**, *22*, 7557.

[36] Wang, X. H.; Gong, Z.; Peng, Y.; Zhang, Y.; Cao, L. M.; Chen, Y. K. An ultra-sensitive and wide strain range sensor via commercial rubber-based 3D hyper-interface and parallel conductive networks. *Adv. Funct. Mater.*, in press, DOI: 10.1002/adfm.202524533.

[37] Castellanos-Gomez, A.; Buscema, M.; Molenaar, R.; Singh, V.; Janssen, L.; Van Der Zant, H. S. J.; Steele, G. A. Deterministic transfer of two-dimensional materials by all-dry viscoelastic stamping. *2D Mater.* **2014**, *1*, 011002.

[38] Henríquez-Guerra, E.; Li, H.; Pasqués-Gramage, P.; Gosálbez-Martínez, D.; D'Agosta, R.; Castellanos-Gomez, A.; Calvo, M. R. Large biaxial compressive strain tuning of neutral and charged excitons in single-layer transition metal dichalcogenides. *ACS Appl. Mater. Interfaces* **2023**, *15*, 57369–57378.

[39] Radatović, B.; Li, H.; D'Agosta, R.; Castellanos-Gomez, A. Giant anisotropic piezoresponse of layered $ZrSe_3$. *Nanoscale Horiz.* **2025**, *10*, 401–408.

[40] Ruano, P. L. A.; Vaquero, D.; Viso, E. S.; Li, H.; Mompeán, F.; Domínguez-Adame, F.; Castellanos-Gomez, A.; Quereda, J. Polarization-sensitive photoresponse in few-layer $ZrSe_3$ photodetectors. *2D Mater.* **2025**, *12*, 015014.

[41] Yip, K. Y.; Wang, L. F.; Poon, T. F.; Yu, K. H.; Lam, S. T.; Lai, K. T.; Singleton, J.; Balakirev, F. F.; Goh, S. K. Shubnikov-de Haas oscillations of biaxial-strain-tuned superconductors in pulsed magnetic field up to 60 T. *APL Mater.* **2024**, *12*, 021124.

[42] Henríquez-Guerra, E.; Almonte, L.; Li, H.; Elvira, D.; Calvo, M. R.; Castellanos-Gomez, A. Modulation of the superconducting phase transition in multilayer 2H–$NbSe_2$ induced by uniform biaxial compressive strain. *Nano Lett.* **2024**, *24*, 10504–10509.

[43] Lan, W. Z.; Fu, P.; Ji, C. Y.; Wang, G.; Yao, Y. G.; Gu, C. Z.; Liu, B. L. Visualization of photonic band structures via far-field measurements in SiN_x photonic crystal slabs. *Appl. Phys. Lett.* **2023**, *122*, 151102.